Modulating calcium phosphate formation using CO_2 laser engineering of a polymeric material

D.G. Waugh and J. Lawrence

School of Engineering, University of Lincoln, Brayford Pool, Lincoln, LN6 7TS, UK.

Corresponding author:
D.G. Waugh
School of Engineering
University of Lincoln
Brayford Pool
Lincoln
LN6 7TS, UK

1.0 – Abstract

The use of simulated body fluid (SBF) is widely used as a screening technique to assess the ability of materials to promote calcium phosphate formation. This paper details the use of CO_2 laser surface treatment of nylon® 6,6 to modulate calcium phosphate formation following immersion in SBF for 14 days. Through white light interferometry (WLI) it was determined that the laser surface processing gave rise to maximum Ra and Sa parameters of 1.3 and 4.4 μm, respectively. The use of X-ray photoelectron spectroscopy (XPS) enabled a maximum increase in surface oxygen content of 5.6 %at. to be identified. The laser-induced surface modifications gave rise to a modulation in the wettability characteristics such that the contact angle, θ, decreased for the whole area processed samples, as expected, and increased for the patterned samples. The increase in θ can be attributed to a transition in wetting nature to a mixed-state wetting regime. It was seen for all samples that calcium phosphate formed on each surface following 14 days. The largest increase in mass, Δg, owed to calcium phosphate formation, was brought about by the whole area processed sample irradiated with a fluence of 51 Jcm^{-2}. No correlation between the calcium phosphate formation and the laser patterned surface properties was determined due to the likely affect of the mixed-state wetting regime. Strong correlations between θ, the surface energy parameters and the calcium phosphate formation for the whole area processed samples allow one to realize the potential for this surface treatment technique in predicting the bone forming ability of laser processed materials.

Keywords: CO_2 laser, surface treatment, simulated body fluid, calcium phosphate formation, bioactivity.

2.0 – Introduction

With an ageing population there is an ever increasing demand for biological implants [1]. These needs have to be significantly met so that costs and the need for unnecessary surgery are considerably reduced. Consequently, it is imperative for the biomedical industry to develop a cost-effective method to manufacture cheap implants which can be used in confidence to ensure a dramatic reduction in failure rates. Surface treatment techniques currently available within the bio-technology industry for surface modification are somewhat limited and expensive, involving numerous processing steps [2-5]. This will have a major impact upon the industry insofar as it will hinder expansion and seriously limit the applications for polymers due to insufficient surface properties. Lasers offer a unique means of surface treatment in that they can accurately modify a number of surface parameters simultaneously leaving the bulk unchanged. Previous work has

shown that these laser-induced surface modifications have a relationship with the wettability characteristics for nylon® 6,6 [6,7]. Furthermore, it has been evidenced that there is a relationship between the wettability characteristics and bioactive nature of the nylon® 6,6 in terms of osteoblast cell growth [8].

Nylon® 6,6 has been used for such biological applications as sutures, tracheal tubes and gastrointestinal segments [9]. With regards to orthopaedic applications it can be seen that nylon® is not commonly employed due to the hygroscopic nature having a large affect on the mechanical properties over long periods of time [10]. Having said that, the use of nylon® 6,6 within this work gives high value experimentally insofar as to ascertain generic factors for polymeric materials which could be used to predict the biofunctionality. Also, by modifying the surface of polymeric materials it may be possible, in the future, to identify other biological applications. On account of nylon® 6,6 being a relatively inexpensive polymer when compared to other polymer types, by identifying other applications for this material the biological industry would benefit by being able to implement cheaper, more economic bio-implant materials.

It is crucial that the bioactivity of the materials employed is sufficient in order to ensure that the failure rate of the implants is kept to a minimum. This can be done by ensuring that, through extensive testing methods, a biomaterial incites adequate cell adhesion and proliferation to allow for the biological environment to accept the biomimetic material. It is essential for implants to be accepted and integrated into the biological environment as quickly as possible as increased integration time would give rise to the possibility of common clinical problems such as loss of tissue in the vicinity of the implant or the implant becoming loose allowing for discomfort or pain to the patient [11]. As a result of this, in order to achieve the best possible results from a polymeric biomaterial a range of skills are required that span over multiple disciplines. As such, throughout the research of many over this multi-disciplinary subject it has been realized that both the bulk and surface properties of all biomaterials hold the ability to influence the degree of bioactivity [8,12-14].

Simulated body fluid (SBF) is a metastable calcium phosphate solution with an ion concentration approximately equivalent to that of human blood plasma. It is widely accepted as a screening technique to assess the bone forming potential of materials [15]. This is owed to the fact that the bioactivity of almost all orthopaedic biomaterials has a strong relationship with the ability of that material to promote the formation of bone-like carbonite apatite crystals [16-18]. What is more, this apatite layer associates specific bone proteins which are crucial for any form of bone reconstruction [19].

It should also be noted that, like many *in vitro* experiments, employing SBF does not fully reproduce the *in vivo* environment for bone formation and may produce misleading results. But, as stated by Roach [15], *in vitro* techniques using SBF allows one to conduct rapid screening for bone formation. As a result, this paper details a study involving the affects of CO_2 laser surface treatment of nylon® 6,6 on calcium phosphate formation following submersion in SBF. Furthermore, generic surface parameters and wettability characteristics are discussed which are believed to have the potential to give the ability of predicting the bioactive nature of the given material.

3.0 – Experimental Technique

3.1 – Nylon® 6,6 Material

The nylon® 6,6 (T_m: 255°, ρ: 1.3 gcm^{-3}) was sourced in 100 mm^2 sheets with a thickness of 5 mm (Goodfellow Cambridge, Ltd). To obtain a conveniently sized sample for experimentation the as-received nylon® sheet was cut into 20 mm diameter discs using a 1 kW continuous wave (cw) CO_2 laser (Everlase S48; Coherent, Ltd). No discernible heat affected zone (HAZ) was observed under optical microscopic examination.

3.2 – Laser Processing Procedures

3.2.1 – CO_2 Laser-Induced Patterning

In order to generate the required marking pattern with the 10 W CO_2 laser system (10 W; Synrad, Inc.), Synrad Winmark software version 2.1.0, build 3468 was used. The nylon® 6,6 samples were placed into the laser system onto a stage in which they were held in place using a bracket with a 20.5 mm diameter hole cut into the centre of the bracket. The focal length was 250 mm away from the output facet of the laser system and the system employed a galvanometer scanner to scan the 95 μm spot size beam directly across the stationary target material. It should be noted that the laser processing system was held in a laser safety cabinet in which the ambient gas was air and an extraction system was used to remove any fumes produced during laser processing.

Four patterns were induced onto the surfaces of the nylon® 6,6 samples; these were trenches with 50 μm spacing (CT50), hatch with 50 μm spacing (CH50), trenches with 100 μm spacing (CT50) and hatch with 100 μm spacing (CH100). In addition, an as-received control sample was used (AR). The laser power was set to 70% (7 W) operating at 600 mms^{-1} for each of the irradiated patterns.

3.2.2 – CO_2 Laser Whole Area Irradiative Processing

A cw 100 W CO_2 laser (DLC; Spectron, Ltd) was used to scan a 5mm diameter beam across the target sample with one pass in order to irradiate the test area with an irradiance of 510 Wcm^2. By using a galvanometer, scanning speeds of 150, 100, 75, 50, 25 and 20 mms^{-1} were used to irradiate six samples with effective fluences of 16.84 (samples CWA17), 25.51 (sample CWA26), 34.18 (sample CWA34), 51.02 (sample CWA51), 102.04 (sample CWA102) and 127.55 (sample CWA128) Jcm^{-2}, respectively. As with the laser-induced patterning, experimentation was carried out in a laser safety cabinet in which the ambient gas was air.

3.3 – Topography, Wettability Characteristics and Surface Chemistry Analysis

Following laser surface treatment 3-D profiles were determined for each sample using a white light interferometer (WLI) (NewView 500; Zygo, Ltd) with MetroPro and TalyMap Gold Software. The WLI was set-up using a ×10 Mirau lens with a zoom of ×0.5 and working distance of 7.6 mm. This system also allowed Sa and Ra roughness parameters to be determined for each sample. Sa can be defined as the arithmetic average of the absolute values over the whole of the laser surface treated area and Ra the arithmetic average of the absolute values along a single specified direction.

Prior to any wettability study, the samples were ultrasonically cleaned in isoproponal (Fisher Scientific Ltd., UK) for 3 minutes at room temperature. This was to allow for a relatively clean surface prior to any contact angle, θ, measurements being taken. After that, the samples were dried using a specimen dryer (Metaserv, Ltd., UK). A sessile drop device (OCA20; Dataphysics Instruments, GmbH) was then used with relevant software (SCA20; Dataphysics Intrsuments, GmbH) to allow the recent advancing θ for triply distilled water and diiodomethane to be determined for each sample. Thereafter an OWRK plot was drawn using the advancing θ for the two liquids to determine the surface energy each sample. For the two reference liquids the SCA20 software used the Ström *et al* technique (triply distilled water – SFT(total:72.80), SFT(D:21.80), SFT(P:51.00); diiodomethane – SFT(total:50.80), SFT(D:50.80), SFT(P:0.00)) to calculate the surface energies of the samples. To obtain a statistical mean ten θ, using two droplets in each instance, were recorded for each liquid and surface. By carrying out these measurements the total surface energy, γ^T, and polar component, γ^P, was established for each laser processed nylon® 6,6 sample.

To ascertain any surface modifications in terms of surface oxygen content all samples were analysed using x-ray photoelectron spectroscopy (XPS). Further details of the XPS setup can be found in [20].

3.4 – Simulated Body Fluid (SBF) Procedure

Prior to experimentation all samples and apparatus were autoclaved if not already sourced in sterile packaging. The samples were then placed into sterile 30 ml glass containers, immersed in 30 ml of simulated body fluid (SBF) and placed into an incubator to keep the temperature constant at 37°C for 14 days. The SBF was prepared in accordance with previous work [20].

3.5 – Scanning Electron Microscopy (SEM) and Energy-Dispersive X-Ray Spectroscopy (EDX) of SBF Immersed Samples

Prior to being immersed in the SBF the nylon® 6,6 samples were weighed using a balance (S-403; Denver Instrument, GmbH) which had a readability of 0.001 g. Once the 14 days had elapsed the samples were removed from the SBF, rinsed lightly with distilled water and allowed to air dry in a clean room. Once fully dry the difference in weight, Δg, before and after being immersed in the SBF was determined. The samples were then gold coated and analysed using scanning electron microscopy (SEM). Furthermore, during the SEM analysis the samples were analysed using EDX in order to identify elements present on the surface of the nylon® 6,6 samples following immersion in SBF.

4.0 – Results and Discussion

4.1 – Topography

4.1.1 – CO_2 Laser-Induced Patterning

Through previous work it has been established that the CO_2 laser-material interaction is that of a thermolytical nature which gave rise to melting and resolidification [6,8]. As one would expect, scanning a predetermined pattern across the nylon® 6,6 surfaces gave rise to a significant variation in topography when compared to the as-received sample (AR). This is more apparent when comparing the 3-D profiles and profile extractions of the as-received sample (see Figure 1) and the laser patterned samples (see Figure 2).

From Figure 1 and Figure 2 it can be seen that the CO_2 laser-induced patterned samples had considerably rougher surfaces with the largest peak heights being of the order of 2 μm in contrast to the as-received sample which had peaks heights of up to 0.2 μm. On account of this increase in peak heights for the CO_2 laser-patterned samples the surface roughness (see Table 1) increased considerably with the largest Sa of 0.4 μm being achieved with the 50 μm hatch sample (CH50). It is given in Table 1 that the patterned samples with scan dimensions of 50 μm (samples CT50 and CH50) had larger Sa roughness values when compared to the samples patterned with 100 μm scan dimensions (samples CT100 and CH100). This can be attributed to the fact that the 50 μm scan

dimensions irradiated more of the sample giving rise to an increase of mass being melted and re-solidified. Also, it can be seen from the Table 1 that the roughness for the hatch patterns had decreased in comparison to the trench patterns. This can be explained by the laser re-melting sections of the nylon® 6,6 surface owed to the scanning process of the system. By re-melting these sections the material could then have re-solidified into a smoother surface topography, eradicating the natural periodicity of the initial induced pattern.

The profile extractions shown in Figure 2 indicate that a high level of periodicity arose in the topography for most of the laser patterned samples. Having said that, it is evident that from Figure 2 that the 50 μm patterns (CT50 and CH50) had the least periodicity, which can be attributed to the fact that the beam spot size was 95 μm and consequently allowed the scans to significantly overlap, eliminating the natural periodicity of the original scanned pattern. This would allow one to explain the surface Sa roughness increase as seen in Table 1 as the scanned 50 μm dimensioned patterns (samples CT50 and CH50) had up to a three times larger Sa values compared to the 100 μm scan dimensioned nylon® 6,6 samples (samples CT100 and CH100). Another point of interest which is shown in Figure 2 is that sharp steep gradients arose on account of the CO_2 laser-induced patterning of the nylon® 6,6 samples.

4.1.2 – CO_2 Laser Whole Area Irradiative Processing

From Figure 3 it can be seen that the CO_2 laser whole area irradiative processing of the nylon® 6,6 gave rise to a significantly modified surface, especially with those samples which had been irradiated with large fluences (samples CWA102 and CWA128). This was due to more melting taking place arising from the significantly larger temperature rise owed to the large fluences incident on the nylon® 6,6 surfaces.

Figure 3 also allows one to see that there was further evidence of considerable melting on account of one being able to identify craters left from evolved gases breaking at the surface. This is especially apparent for sample CWA102 and sample CWA128 which had larger incident fluences (see Figure 3(e) and Figure 3(f)). Leading on from this, the extent of melting can be further identified through the profile extractions (see Figure 3) which show that peak heights of 10 to 15 μm was achieved for those samples with incident fluences of 102 and 128 Jcm^{-2} (samples CWA102 and CWA128). It should also be noted here that as the fluence used for samples CWA17 (see Figure 3(a)) and CWA26 (see Figure 3(b)) appeared experimentally to be close to that of the laser-material interaction threshold, qualitatively there did not appear to be significant difference between the topographies observed for them and that of the as-received sample (see Figure 1).

4.2 – Wettability Characteristics and Surface Oxygen Content

4.2.1 – CO_2 Laser-Induced Patterning

Table 1 gives a summary of the results obtained for each of the nylon® 6,6 samples including surface roughness, γ^T, surface oxygen content and θ. Current theory states that for a hydrophilic

material such as nylon® 6,6 an increase in roughness and surface oxygen content should bring about a reduction in θ [12]. However, Table 1 shows that this was not the case for the CO_2 laser-induced patterned samples as θ had increased by up to 10° even though a maximum increase in Sa was determined to be around 0.6 μm when compared to the as-received sample (AR). As hypothesized previously [6,8], this phenomenon can be explained by the existence of a mixed-state wetting regime [21-22] in which both Cassie-Baxter and Wenzel regimes coexist over the material-liquid interface. This mixed-state wetting regime can also account for the observed reduction in apparent γ^P and apparent γ^T with γ^P reducing by up to 8 mJm^{-2} and γ^T reducing by up to 7 mJm^{-2} when compared to the as-received sample (AR) which had γ^P and γ^T values of 17.69 and 47.34 mJm^{-2}, respectively.

Figure 4 shows that θ was to some extent an inverse function of both γ^P and γ^T in which θ reduced on account of an increase in γ^P and γ^T. This is highly significant as even though θ has, in general, increased upon an increase in surface roughness (see Figure 5), γ^P and γ^T must still play an important role in determining the wettability of laser surface modified nylon® 6,6. In terms of surface roughness, Figure 5 shows the correlation observed between θ and the surface roughness parameters Ra and Sa. It can be seen from Figure 5(a) that θ did not appear to have any correlation between Ra; however, Figure 5(b) suggests that an increase in Sa gave rise to an increase in θ up to 0.4 μm. This could be important as it may indicate a transition in wetting regimes on account of how the liquid droplet sits in equilibrium on the rough periodic laser-modified nylon® 6,6 surface.

4.2.2 – CO_2 Laser Whole Area Irradiative Processing

The CO_2 laser whole area irradiative processed samples corresponded with current theory such that the reduction in θ arose from the surface roughness, γ^P and γ^T increasing. Furthermore, From Table 1 it is possible to deduce that θ for sample CWA51 increased in comparison to the as-received sample (AR). This could be on account of the presence of a mixed-state wetting regime as mentioned earlier in Section 4.2.1, even though the surface roughness increased, apparent γ^P decreased and surface oxygen content increased. From Table 1 , in comparison to the as-received sample (AR) the largest decrease of 13° in θ was found to arise from sample CWA128 which had the largest incident fluence of 128 Jcm^{-2}

Also, it has been observed that there was an inverse correlation between γ^P, γ^T and θ. In order to confirm what was observed from the results given in Table 1, Figure 4 shows graphically that following CO_2 laser whole area irradiative processing θ was an inverse function of γ^P and, to some extent an inverse function of γ^T. Following on, further confirmation that these samples corresponded to current theory was determined by Figure 5 which shows that with the exception of sample CWA51 the CO_2 laser whole area irradiative processed samples gave rise to a θ with an inverse function correlation with the surface roughness parameters Ra and Sa.

4.2.3 – Comparison Between CO_2 Laser-Induced Patterning and CO_2 Laser Whole Area Irradiative Processing

Owed to the different processing techniques giving rise to variations in wetting natures for the nylon® 6,6 it is likely that surface oxygen content may not be the main driving force for wettability. This is because the surface oxygen content increased in all instances by up to 2 %at. for the patterned samples and up to 5 %at. for the whole area irradiated samples. The increase in surface oxygen content can be attributed to the thermolytical interaction between the nylon® 6,6 material and the CO_2 laser beam.

Upon analyzing the CO_2 laser-induced patterned surfaces it was found that the γ^T and γ^P had decreased by up to 7 mJm^{-2} and the surface roughness had considerably increased. It was found that γ^P and γ^T for the samples studied were both a decreasing function of the θ, which correlates with current theory; however, current theory states that θ for a hydrophilic surface should decrease upon increasing surface roughness which has not been seen throughout this experimentation.

It is proposed here that a change from the Wenzel regime to a mixed-state wetting regime was the likely reason for the observed increase in θ for the CO_2 laser-induced patterned nylon® 6,6 [22,23] So, the surface roughness along with the induced pattern yielded a water droplet which was held in an intermediate state such that both wetting regimes coexisted .This is a likely explanation as to how an increase in θ and reduction in apparent γ^P was observed for the laser patterned samples and still be hydrophilic. Therefore, in this instance the topographical surface pattern appeared to manipulate the wettability characteristics of the laser surface treated nylon® 6,6. What is more, following whole area irradiative processing an increase in surface roughness, increase in γ^P and γ^T gave rise to a reduction in θ. This further suggests that the induced patterns had a large impact on the wetting regime.

One can see from Figure 4 that θ was an inverse function of both γ^P and γ^T when collating the results for the CO_2 laser-induced patterned samples and CO_2 laser whole area irradiative processed samples. This allows one to identify that all samples corresponded to the theory that an increase in surface energy components gives rise to a reduction in θ even though an increase in θ was observed for the CO_2 laser-induced patterned nylon® 6,6 samples.

Figure 5 shows that there did not seem to be any specific correlation between θ and the surface roughness parameters. This is on account of the samples with Ra and Sa values slightly higher than the as-received sample (AR), between 0 and 1 μm, giving rise to an increase in θ of up to 15°. This can be primarily seen to be on account of the CO_2 laser-induced patterned samples in which a mixed-state wetting regime likely occurred to give an increase in θ even though a reduction in surface energy components and an increase in surface roughness was observed.

4.3 – Calcium Phosphate Formation

4.3.1 – CO_2 Laser-Induced Patterning

Following immersion in SBF only a very small amount of sediment was present on the as-received sample (see Figure 6(a)) in comparison to the other samples which had undergone CO_2 laser-induced patterning (see Figures 6(b) to (e)). It is also apparent from Figure 6(b) and 6(e) that the sediment preferentially formed around craters which arose due to evolved gases breaking at the surface during the melting. This highlights that it may be possible to construct a polymeric surface which allows selective calcium phosphate formation giving rise to selective positioning for the growth of osteoblast cells.

It is also significant to note that each of the CO_2 laser-induced samples and as-received sample (AR) gave rise to an increase in mass which can be attributed to the formation of the sediment which was identified in Figure 6. Figure 7 shows that the CO_2 laser-induced patterned nylon® 6,6 samples (CT50, CT100, CH50 and CH100) gave rise to a larger increase mass when compared to the as-received sample (AR) by up to 0.015 g. Furthermore, Figure 7 shows that the increase in mass for all of the CO_2 laser-induced patterned samples was around 0.026 g which suggests that in terms of calcium phosphate formation there was no difference between any of the CO_2 laser-induced patterned nylon® 6,6 samples.

4.3.2 – CO_2 Laser Whole Area Irradiative Processing

Figure 8 shows the SEM micrographs for the CO_2 laser whole area processed samples, allowing one to see that more sediment adhered to the surface when compared to the as-received sample (see Figure 8(a)). When comparing the CO_2 laser whole area irradiative processed samples on their own it can be seen from Figure 8(e) and Figure 8(f) that the samples irradiated with the largest fluences of 102 and 128 Jcm^{-2} (CWA102 and CWA128) appeared to give rise to calcium phosphate preferentially forming around the craters that arose from the laser processing.

Figure 7 shows a histogram of the difference in mass, Δg. For the CO_2 laser whole area irradiative processed samples this confirms that Δg increased considerably when compared to the as-received sample (AR). The increase in mass for the CO_2 laser whole area irradiative processed samples had increased by at most 0.05 g with the as-received sample giving an increase in mass of only 0.018 g. Another factor which can be taken from Figure 7 is that the increase in mass steadily increased from sample CWA17 to sample CWA51which gave the largest increase in mass of 0.05 g in comparison to the other CO_2 laser whole area irradiative processed samples. This could be noteworthy as it suggests that an operating window to give the most optimum calcium phosphate formation is possible owed to the fact that fluences greater than 51 Jcm^{-2} (sample CWA102 and CWA128) gave the lowest increase in mass of 0.03 and 0.025 g, respectively.

4.3.3 – Comparison Between CO_2 Laser-Induced Patterning and CO_2 Laser Whole Area Irradiative Processing

It has been confirmed from Figure 6 and Figure 8 that calcium phosphate, following immersion of the samples in SBF for 14 days, formed on all of the nylon® 6,6 samples studied. Visually, it can also be

seen that more sediment had formed upon the CO_2 laser whole area irradiative processed samples. What is more, with those samples which had craters formed as a result of the evolved gases the sediment appeared to be preferentially forming around them. This is a very interesting result as it suggests that both of the CO_2 laser processing techniques could be implemented for processing nylon® 6,6 samples for selective osteoblast cell growth.

From Figure 7 it can be seen that the CO_2 laser whole area irradiative processed nylon® 6,6 samples gave rise to a more enhanced calcium phosphate layer response insofar as there was more sediment present following 14 days of immersion in SBF which inherently gave rise to a significant increase in mass. With regards to the CO_2 laser-induced patterned samples it was found that there was an equivalent mass increase for all samples of around 0.03 g. In contrast, the CO_2 laser whole area irradiative processed samples gave a more modulated response in that the difference in mass increased steadily up to 0.05 g as a result of larger incident fluences until 51 mJm^{-2}, beyond which Δg reduced which was similar to that of the CO_2 laser-induced patterned samples. On account of the larger increase in mass for most of the CO_2 laser whole area irradiative processed samples it is reasonable to say that the compared to the as-received sample (AR) and the CO_2 laser-induced patterned samples, the CO_2 laser whole area irradiative processed samples gave rise to a more biomimetic nylon® 6,6 surfaces allowing for a more sufficient surface for osteoblast cell growth and proliferation. In addition to this, it is possible to deduce from Figure 7(a) that there appeared to be a potential threshold fluence between 51 and 102 Jcm^{-2} beyond which the calcium phosphate formation was less enhanced compared to the other CO_2 laser whole area irradiative processed samples.

Figure 9 shows the surface elemental data for the as-received sample (AR) and a typical CO_2 laser surface modified, indicating that phosphorous and calcium was present on the surface of the nylon® 6,6 samples, following the formation of the calcium phosphate. This is of importance due to phosphorous and calcium having to be present which would inherently increase the bioactivity of the material in terms of bone-bonding ability.

4.3.4 – Wettability Characteristics and Surface Parameters

Figure 7(a) shows a histogram of the increase in mass for each sample in relation to θ. In terms of θ it can be said that for all of the CO_2 laser-induced patterned nylon® 6,6 samples there did not appear to be any correlation between the sediment formation and θ. This could be owed to the transition in wetting regime, as discussed in Section 4.2, playing a significant role in the biomimetic nature of the nylon® 6,6 samples. On the other hand, the CO_2 laser whole area laser irradiative processed samples shown in Figure 7(a) corresponded somewhat to the variation in θ. Since, for those samples with incident fluences between 17 and 51 Jcm^{-2} (CWA17, CWA26, CWA34 and CWA51) an increase in θ gave rise to an increase in Δg. Beyond the fluence of 51 Jcm^{-2} it was found that upon a decrease in θ the increase in Δg became considerably less for sample CWA102 and CWA128. This could be accounted for by the nylon® 6,6 becoming too hydrophilic or too toxic. That is, materials that are too hydrophilic are well known for their cell-repellant properties and hinder the initial protein adsorption needed for a positive cell response [23,24]. Another explanation for this observed phenomenon can be

attributed to a potential increase in surface toxicity whilst oxidation took place during the laser surface treatment. This is on account of the nylon® 6,6 potentially becoming excessively toxic through degradation of the nylon® 6,6 surface giving rise to toxic substances which could hinder the formation of calcium phosphate [25,26].

The relationship between θ and increase in Δg can be further seen in Figure 7(b) if one was to neglect those data points from the as-received sample and CO_2 laser-induced patterned samples (data points between 55 and 67° with Δg values of between 0.01 and 0.03 g). By neglecting these data points one can see that for the CO_2 laser whole area irradiative processed samples gave a positive correlation in which an increase in θ gave a linear increase in Δg. By taking into account those data points plotted for the as-received sample and CO_2 laser-induced patterned samples it can be seen from Figure 7(a) that for the entire CO_2 laser processed samples there was not a correlation between θ and increase in Δg. This indicates that on account of the different surface processing techniques there are different driving parameters for the biomimetic nature of the nylon® 6,6 material irrespective of the fact that the same wavelength was implemented to carry out both of the surface processing in this instance.

From Figure 10(a) one can see that there was no correlation between Δg for the CO_2 laser-induced patterned samples and γ^P which can be attributed to the differences in wetting regime as discussed in Section 4.2. With regards to the CO_2 laser whole area irradiative processed samples it can be seen that for these samples there was a correlation between the observed increase in mass and variation in γ^P. Since, Δg increased upon a reduction in γ^P and can be further confirmed using Figure 10(b) if the as-received and CO_2 laser-induced patterned sample data points were neglected (data points of γ^P between 10 and 20 mJm^{-2} with Δg values of below 0.03 g). Upon neglecting these data points it is possible to ascertain that for the CO_2 laser whole area irradiative processed samples the increase in Δg was a reducing linear function of the measured γ^P. What is more, as discussed previously with regards to θ, this none correlation between γ^P and the increase in mass for the entire CO_2 laser processed samples indicates that the emphasis of biomimetic properties may be on surface processing technique rather than the laser wavelength used.

Figure 11(a) shows that in terms of the increase in mass for the entire CO_2 laser processed samples there was no correlation between γ^T and Δg. This is on account of the CO_2 laser-induced patterned samples giving equivalent increases in Δg even though a variation in γ^T was observed. Also, the none correlation can be accounted for by the fact that the CO_2 laser whole area irradiative processed samples did not follow the trend in that an increase in γ^T upon an increase in incident fluence did not elicit a similar response for Δg as was seen in terms of θ and γ^P. With this in mind, it can be stated that for the CO_2 laser processed samples γ^T may not a dominating parameter in terms of biomimetic nature.

Figure 12(a) gives the relationship between the surface oxygen content and the measured Δg for the entire CO_2 laser processed samples and shows that like for all of the other surface parameters and wettability characteristics, the CO_2 laser-induced patterned samples did not correlate to any trend with the rise in surface oxygen content. As discussed previously this could be on account of the different

wetting regime present which was shown in Section 4.2. Also, in terms of the CO_2 laser whole area irradiative processed samples, Figure 12(a) allows one to see that for samples CWA17, CWA26, CWA34 and CWA51 there is a strong correlation between an increase in surface oxygen content and an increase in Δg. Furthermore, with fluences larger than 51 Jcm^{-2} (sample CWA102 and sample CWA128) it was found that Δg reduced on account of the increase in surface oxygen content. However, this may not be directly related to surface oxygen content as the reduced biomimetic nature for sample CWA102 and sample CWA128 could be accounted for by the nylon® 6,6 becoming too hydrophilic or too toxic as discussed earlier.

It should also be noted here that no correlation was identified between the surface roughness and Δg for all samples. This indicates that the surface roughness was not a dominant parameter governing laser surface treated nylon® 6,6 biofunctionality. Having said that, by identifying specific trends between the wettability characteristics and Δg the laser whole area processed samples, this specific processing technique holds the most potential to be employed in order to allow one to predict the bioactive characteristics.

5.0 – Conclusions

Through CO_2 laser surface processing it has been seen that by employing two different techniques, namely patterning and whole area processing, the wettability characteristics can be significantly modified. For instance the whole area processed nylon® 6,6 samples corresponded with current theory in that θ decreased upon increasing surface roughness. In contrast, the laser-induced patterned samples gave rise to an increase in θ even though an increase in surface roughness was observed. This can be attributed to an intermediate mixed Cassie-Baxter/Wenzel regime, in which both Wenzel and Cassie-Baxter regimes arise at the solid-liquid interface as a result of the formation of the water droplet on the various laser modified surface topographies.

Following immersion in SBF for 14 days it was observed that all CO_2 laser processed samples gave rise to the formation of calcium and phosphorous containing sediment. An increase in Δg of up to 0.015 and 0.024 g was observed for the CO_2 laser-induced patterned and whole area processed samples, respectively, when compared to the as-received sample which had a total increase Δg of 0.016 g. The increase in the formation of sediment indicated that the laser surface treated samples could possess more bone bonding formation potential, allowing for a surface that would enhance osteoblast cell adhesion and proliferation. Leading on from this, it was found that there were different correlative trends observed for the each of the laser processes between mainly θ and γ^P. For the CO_2 laser whole area irradiative processing it was seen that Δg was both an increasing function of θ and a decreasing function of γ^P. Also, the laser-induced patterned samples did not give rise to any distinct correlative trend with Δg, which can be attributed to the likely mixed-state wetting regime giving rise to erroneous results.

On account of the trends identified for the whole area processed nylon® 6,6 samples it can be said that this surface engineering technique has potential to be employed in regenerative medicine to

predict how a given laser surface treated material is going to perform in a given biological environment.

6.0 – Acknowledgements

We would like to thank our collaborators Directed Light Inc., East Midlands NHS Innovation Hub, Nobel Biocare and Photomachining Inc. for all of their much appreciated support. The authors greatly acknowledge the Access to Research Equipment Initiative funded by the EPSRC, (grant number EP/F019823/1). This study was also financially supported by the EPSRC, (grant number EP/E046851/1).

7.0 – References

1. K. MacGregor, The ageing population: U.K. focus for biomedical engineering - policy briefing. The Royal Academy of Engineering 2010.

2. R.S. Benson RS, Use of radiation in biomaterials science, Nucl. Inst.Meth. Phys. Res. B 191 (2002) 752-757.

3. F. Arefi-Khonsari, M. Tatoulian, F. Bretagnol, O. Bouloussa, F. Rondelez, Processing of polymers by plasma technologies, Surf. Coat. Technol. 200 (2005) 14-20.

4. D. Pappas, A. Bujanda, J.D. Demaree, J.K. Hirvonen, W. Kosik, R. Jensen et al., Surface modifcation of polyamide fibers and films using atmospheric plasmas, Surf. Coat. Technol. 201 (2006) 4384-4388.

5. E.M. Harnett, J. Alderman, T. Wood, The surface energy of various biomaterials coated with adhesion molecules used in cell culture, Coll. Surf. B 55 (2007) 90-97.

6. D.G. Waugh, J. Lawrence, C.D. Walton, R.B. Zakaria, On the effects of using CO_2 and F_2 lasers to modify the wettability of a polymeric biomaterial, J. Opt. Laser Technol. 42 (2010) 347-356.

7. D.G. Waugh, J. Lawrence, On the use of CO2 laser induced patterns to modify the wettability of poly(methyl methamecrylate) (PMMA). Opt. Lasers Eng. 48 (2010) 707-715.

8. D.G. Waugh, J. Lawrence, D.J. Morgan, C.L. Thomas, Interaction of CO_2 laser-modified nylon with osteoblast cells in relation to wettability, Mater. Sci. Eng. C 29 (2009) 2514-2524.

9. S.R. Paital, N.B. Dahotre, Calcium phosphate coatings for bio-implant applications: Materials, performance factors and methodologies, Mater. Sci. Eng. R 66 (2009) 1-70.

10. J.J. Rajesh, J. Bijwe, B. Venkataraman, U.S. Tewari, Effect of water absorption on erosive wear behaviour of polyamide, J. Mater. Sci. 37 (2002) 5107-5113.

11. D.C. Giliberti, K.K. White, K.C. Dee, Control of Cell-Biomaterial Interactions, In: S. Dumitriu (editor), Polymeric Biomaterials. Second ed., Marcel Dekker, New York, USA, 2002. p.361.

12. L. Hao, J. Lawrence, Laser Surface Treatment of Bio-Implant Materials, John Wiley & Sons Inc., New Jersey, USA, 2005.

13. B.D. Ratner, Introduction to Testing Biomaterials, In: B.D. Ratner (editor) Biomaterials Science. Second ed., Elsevier Academic Press, San Diego, California, USA, 2004 p.355.

14. J. Black, Biological Performance of Materials: Fundamentals of Biocompatibility, Fourth ed., CRC Press, Florida, USA, 2006.

15. P. Roach, D. Eglin, K. Rohde, C.C. Perry, Modern biomaterials: a review-bulk properties and implications of surface modifications, J. Mater. Sci. Mater. Med. 18 (2007) 1263-1277.

16. W. Song, Y.K. Jun, Y. Han, S.H. Hong, Biomimetic apatite coatings on micro-arc oxidzed titania. Biomaterials 25 (2004) 3341-3349.

17. L. Hao, J. Lawrence, L. Li, The wettability modification of bio-grade stainless steel in contact with simulated physiological liquids by the means of laser irradiation, Appl. Surf. Sci. 247 (2005) 453-457.

18. M. Nagano, T. Kitsugi, T. Nakamura, T. Kokubo, M. Tanahashi, Bone bonding ability of an apatite-coated polymer produced using a biomimetic method: A mechanical and histological study *in vivo*, J. Biomed. Mater. Res. 31 (1996) 487-494.

19. C. Rey, Orthopedic biomaterials, bioactivity, biodegradation; a physical-chemical approach, J. Biomech. 31 (1998) 182-182(1).

20. D.G. Waugh, J. Lawrence, The enhancement of biomimetic apatite coatings by means of KrF excimer laser surface treatment of nylon 6,6. Lasers in Engineering 21 (2011) 95-114.

21. X. Chen, T. Lu, The apparent state of droplets on a rough surface, Sci. China Ser. G-Phys. Mech. Astron. 52 (2009) 233-238.

22. X. Wu, L. Zheng, D. Wu, Fabrication of superhydrophobic surfaces from microstructured ZnO-based surfaces via a wet-chemical route, Langmuir 21 (2005) 2665-2667.

23. M.C. Lensen, V.A. Schulte, J. Salber, M. Diez, F. Menges, M. Moller, Cellular response to novel, micropatterned biomaterials, Pure Appl. Chem. 80 (2008) 2479-2487.

24. M.S. Kim, G. Khang, H.B. Lee, Gradient polymer surfaces for biomedical applications, Prog. Polym. Sci. 33 (2008) 138-164.

25. Sigma-Aldrich. Nylon 6,6 Material Safety Data Sheet - Version 3.0. 2008.

26. S.D. Cook, J.P. Ryaby, J.R.N. McCabe, J.J. Frey, J.D. Heckman, T.K. Kristiansen, Acceleration of tibia and distal radius fracture healing in patients who smoke, Clin. Orth. Rel. Res. 337 (1997) :198-207.

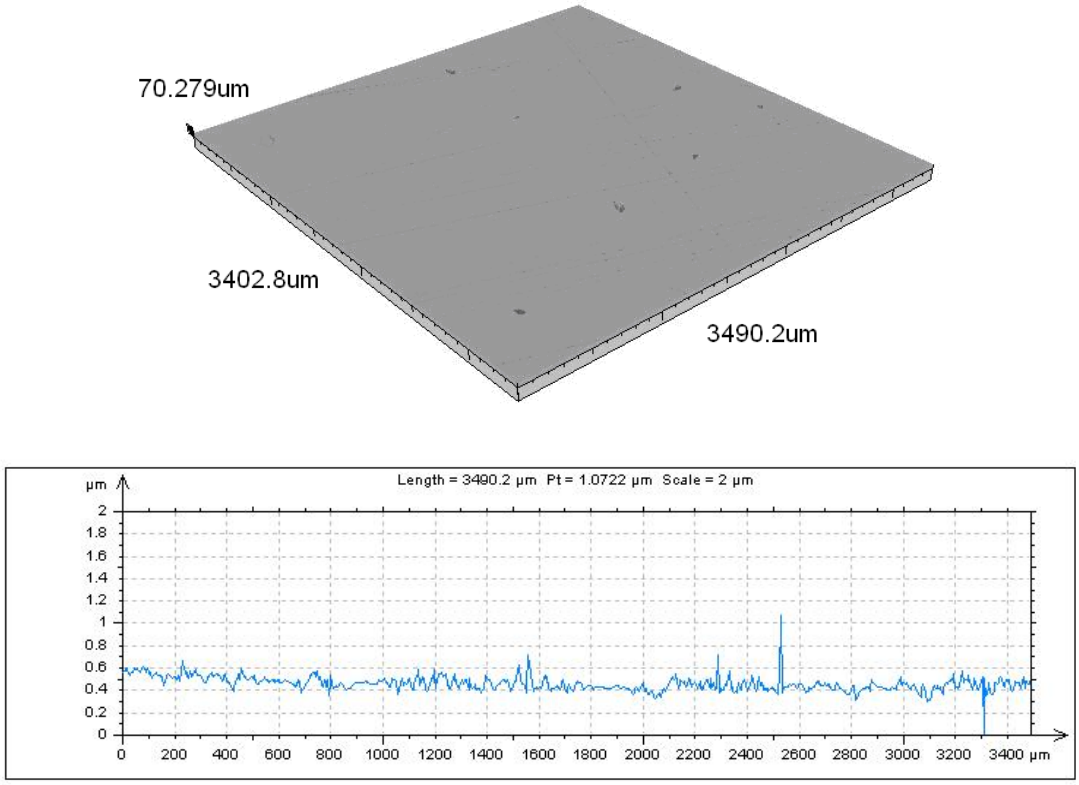

Figure 1 – Continuous axonometric 3-D image and profile extraction for the as-received sample (AR).

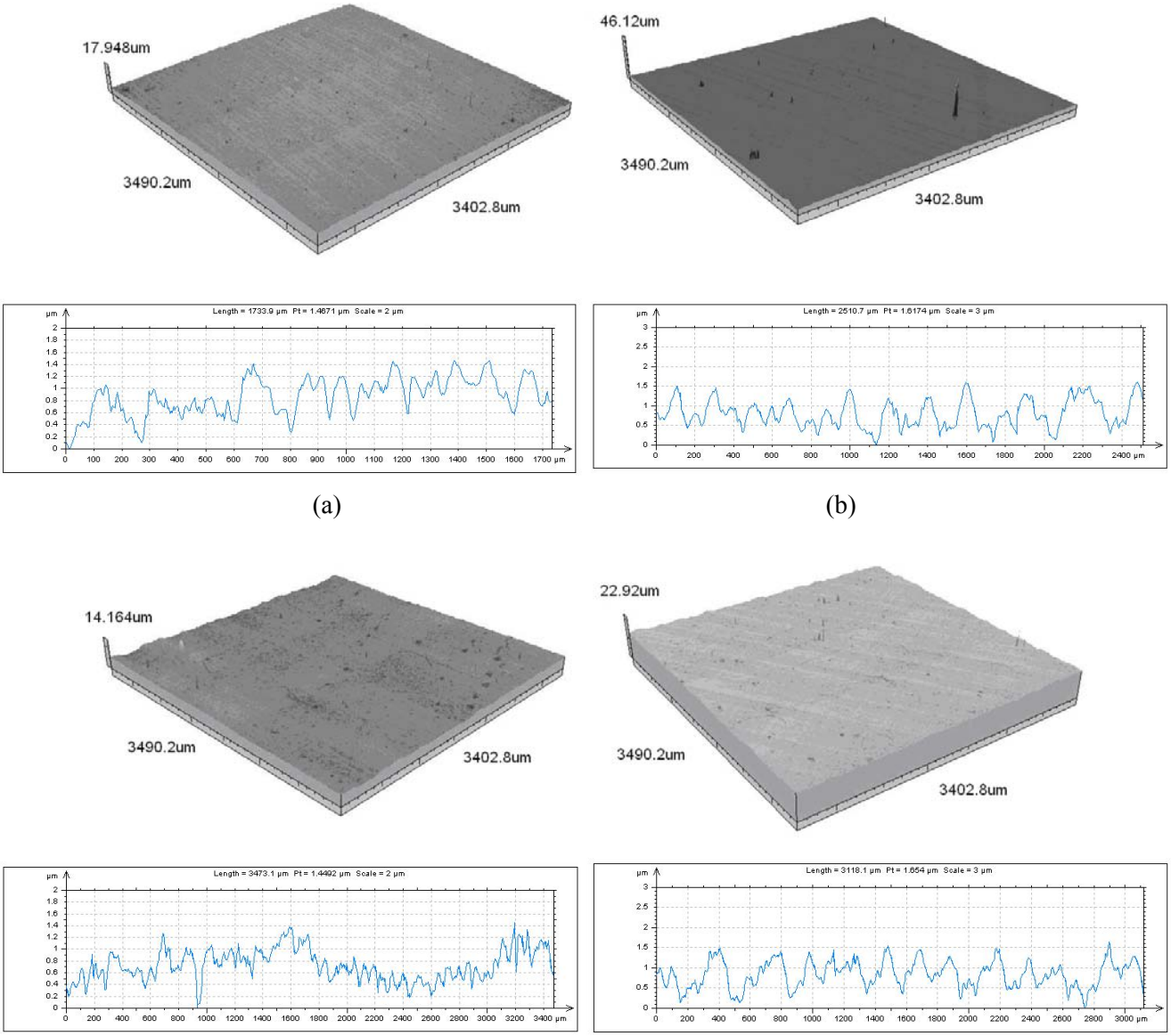

Figure 2 – Continuous axonometric 3-D images for (a) CT50 (b) CT100 (d) CH50 and (d) CH100.

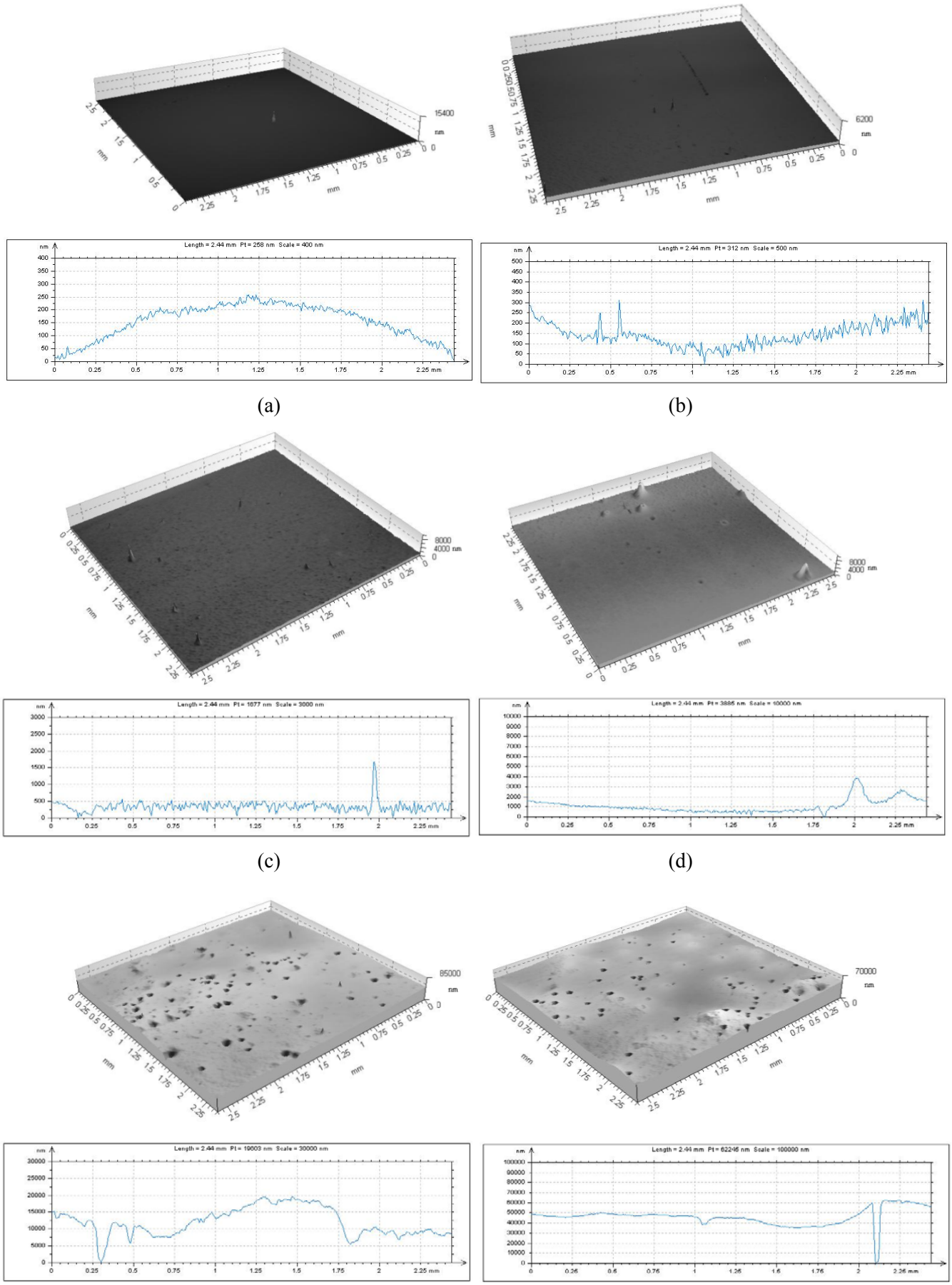

Figure 3 – Continuous axonometric images of samples (a) CWA17, (b) CWA26, (c) CWA34, (d) CWA51, (e) CWA102 and (f) CWA128.

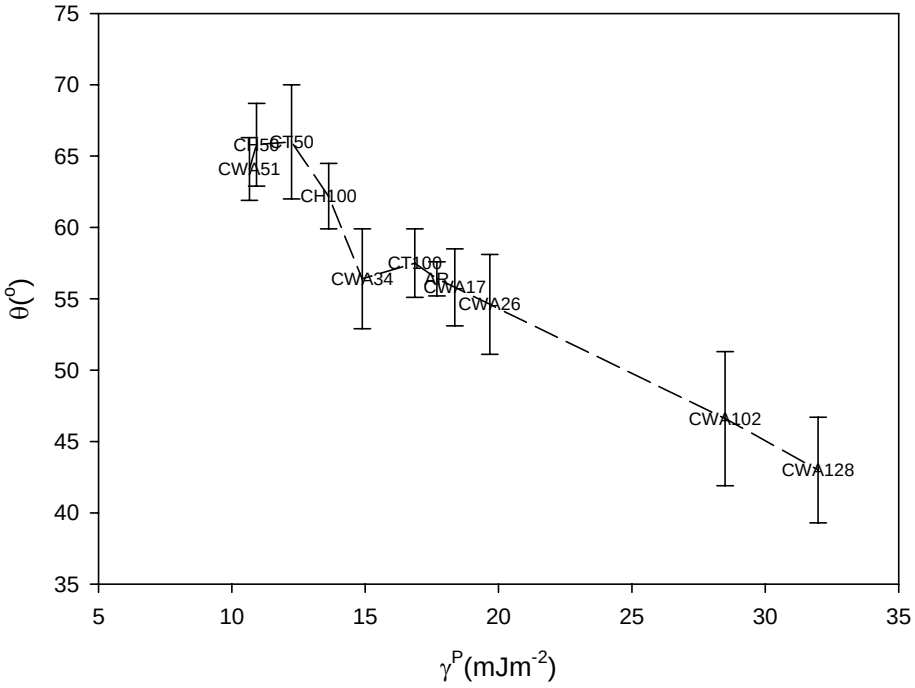

(a)

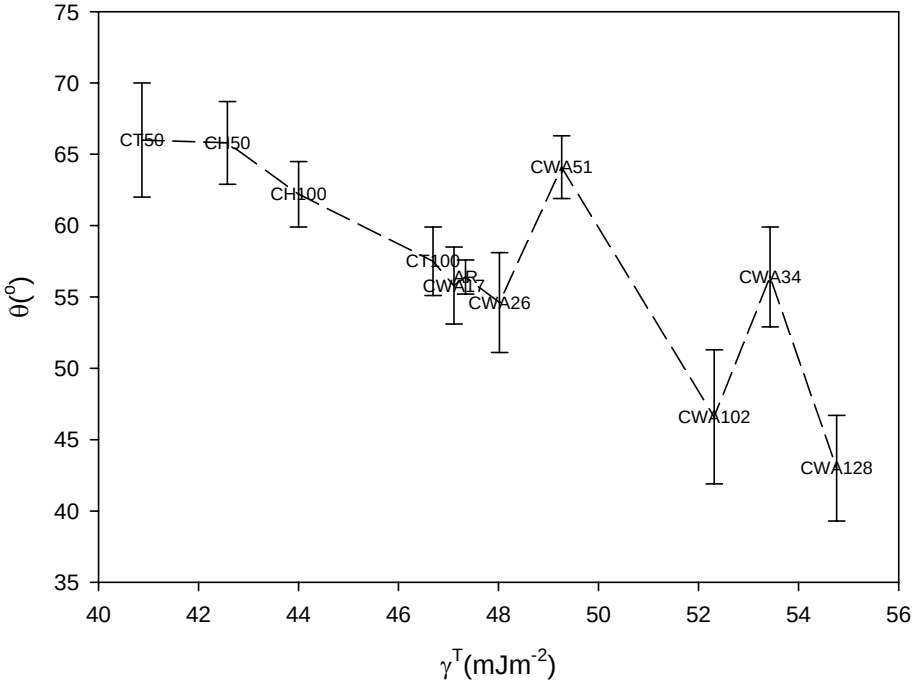

(b)

Figure 4 – Graphs showing the correlation between θ and (a) γ^P and (b) γ^T.

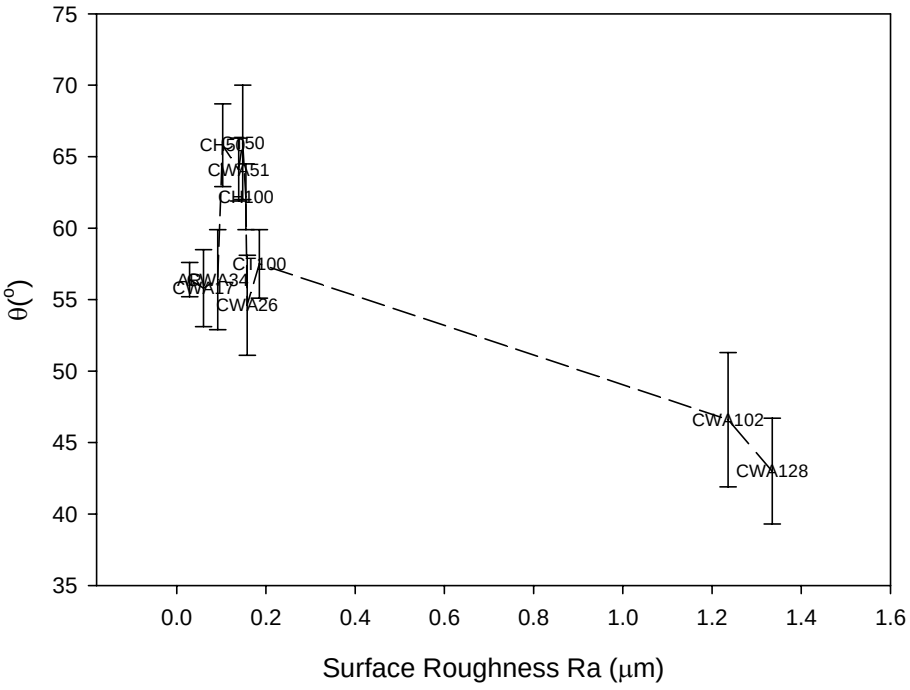

(a)

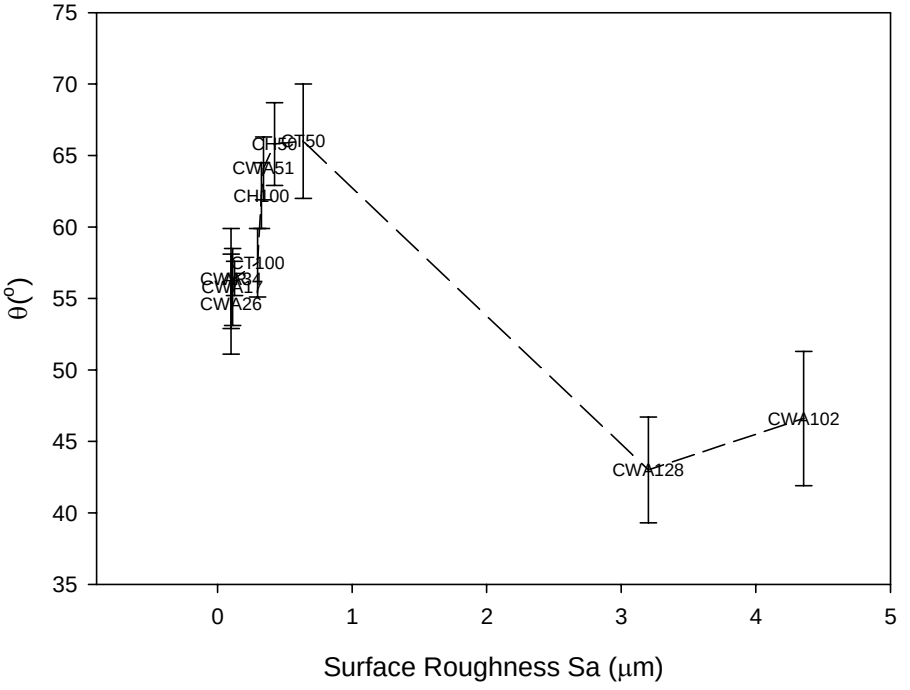

(b)

Figure 5 – Graphs showing the correlation between θ and (a) Ra and (b) Sa.

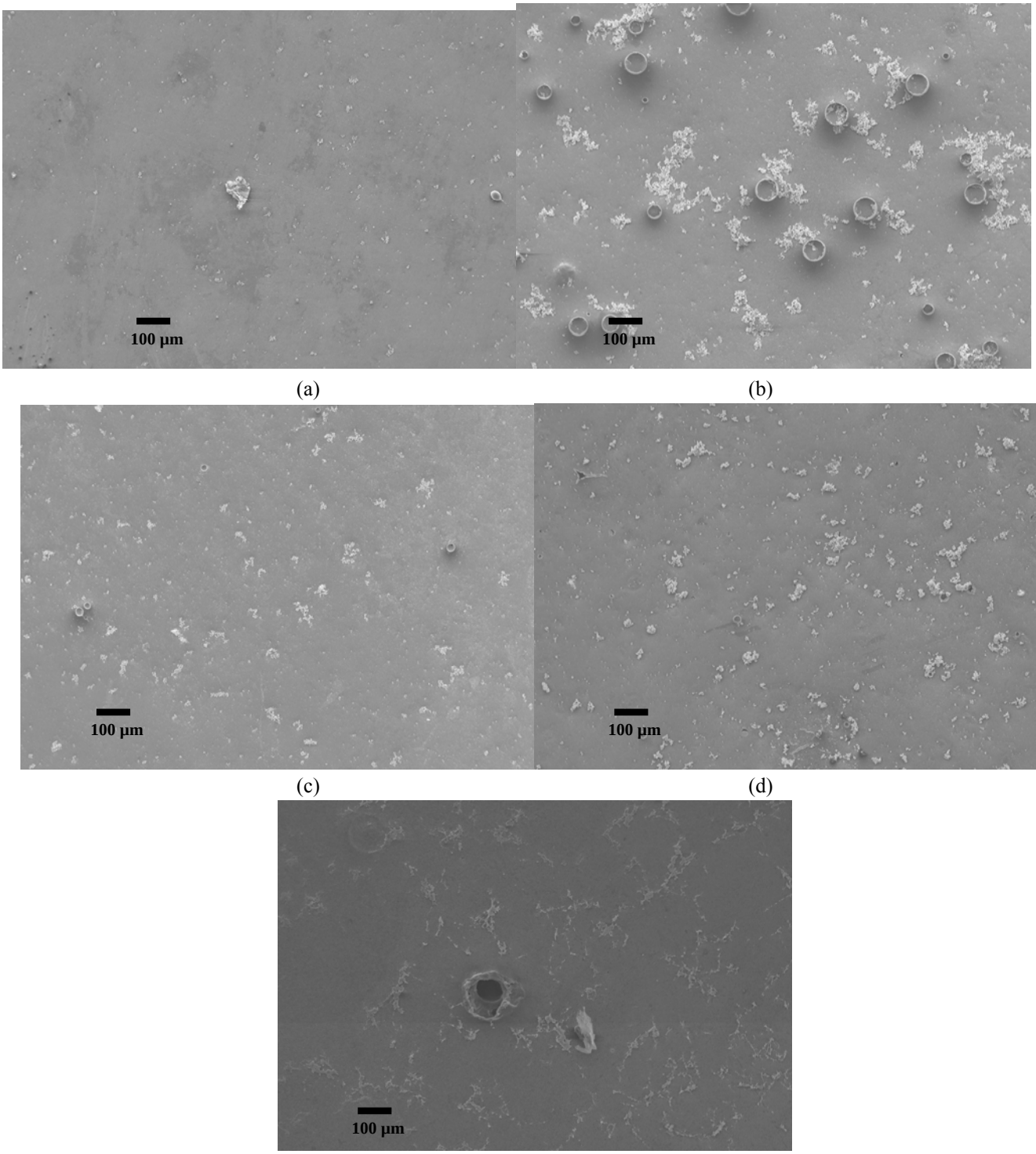

Figure 6 – SEM micrographs for (a) AR, (b) CT50, (c) CT100, (d) CH50 and (e) CH100 after immersion in SBF for 14 days.

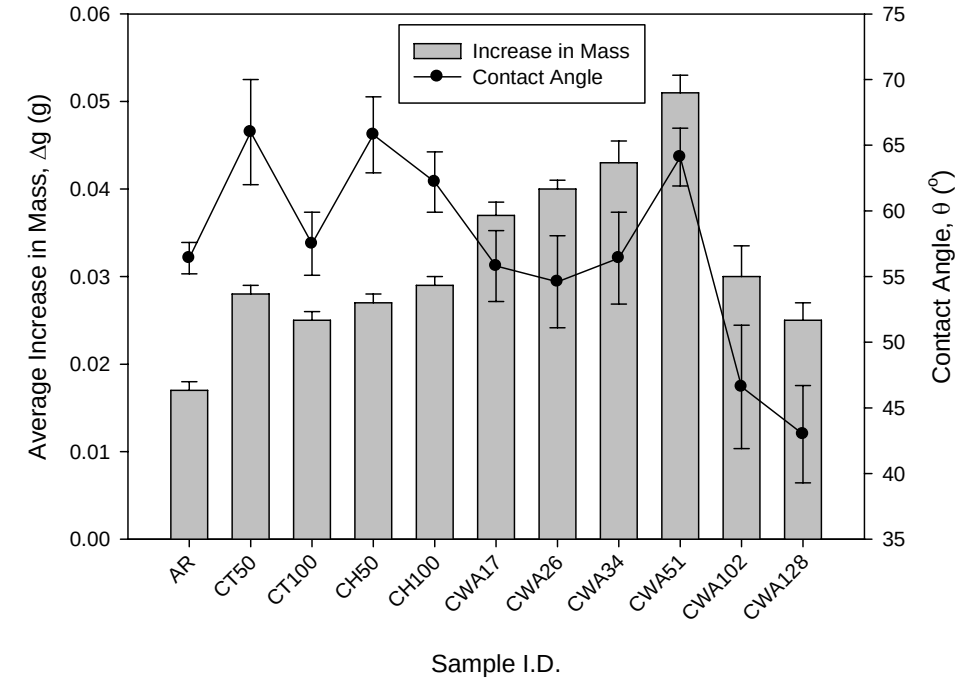

(a)

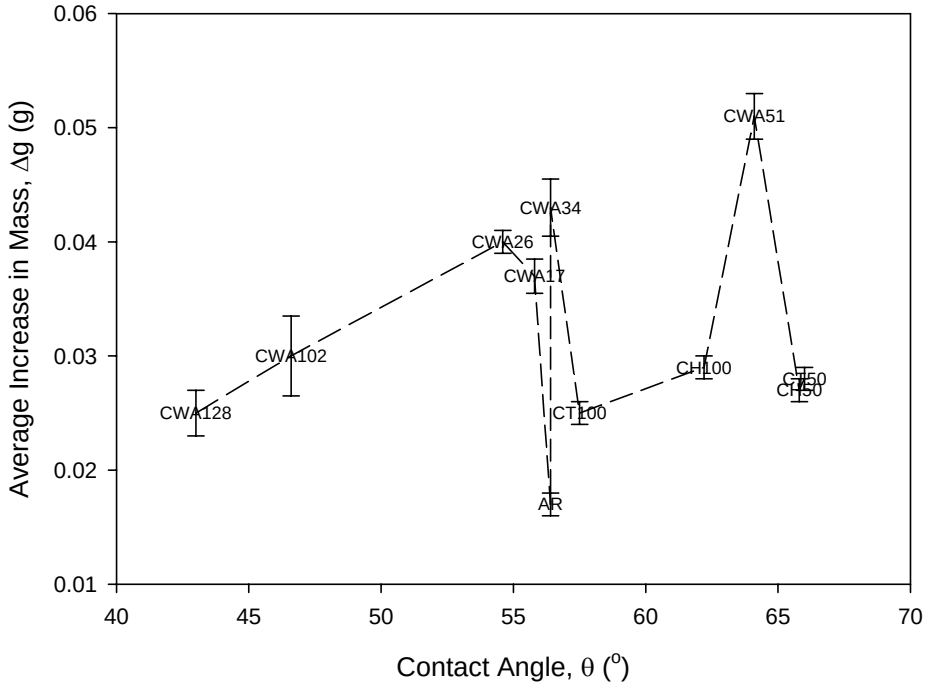

(b)

Figure 7 – (a) Histogram showing the difference in mass before and after immersion in SBF for all CO_2 laser processed samples in relation to θ, (b) Graph showing the relationship between Δg and θ.

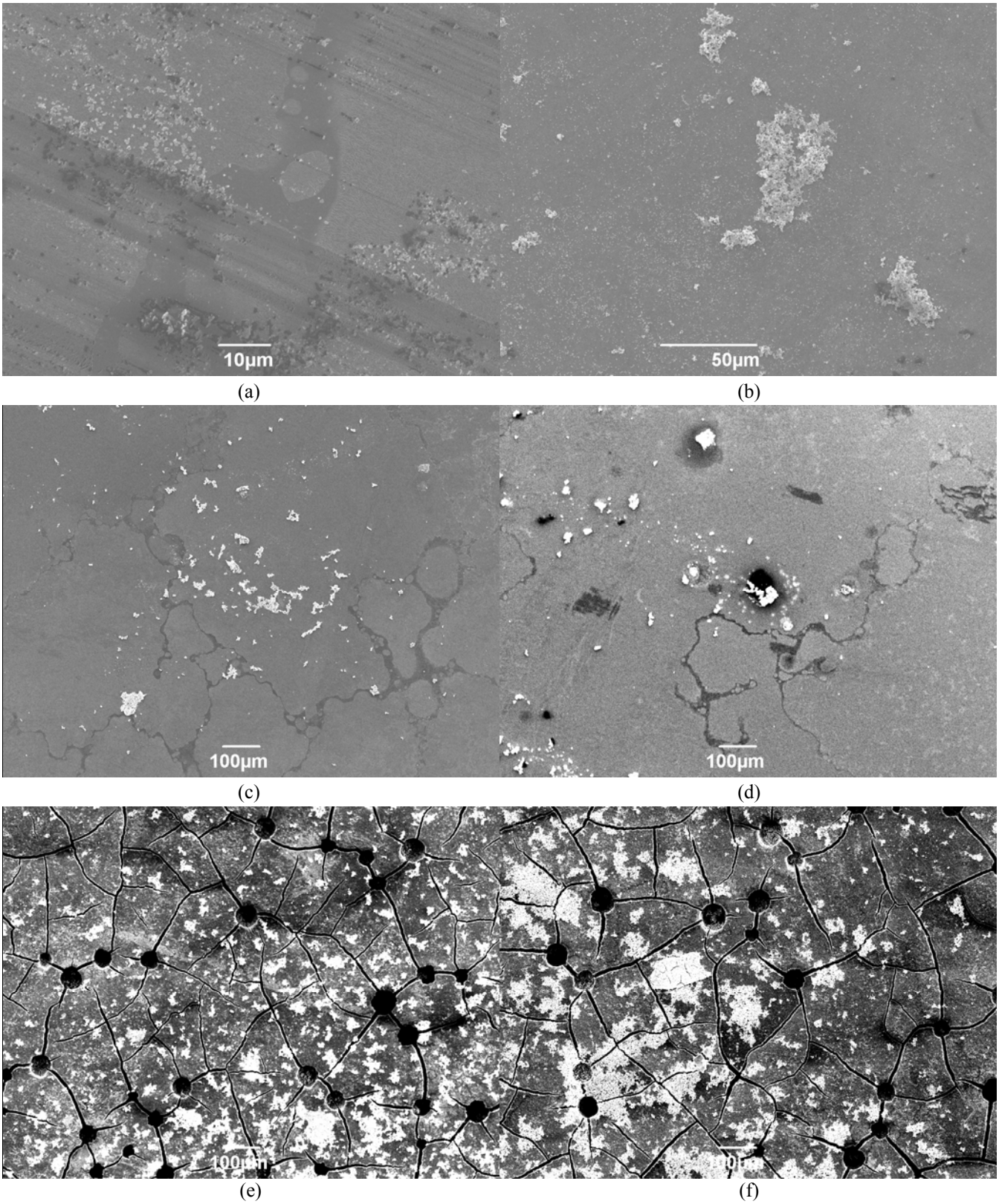

Figure 8 – SEM micrographs showing the SBF apatite formation on the whole area CO_2 laser processed samples (a) CWA17, (b) CWA26, (c) CWA34, (d) CWA51, (e) CWA102 and (f) CWA128.

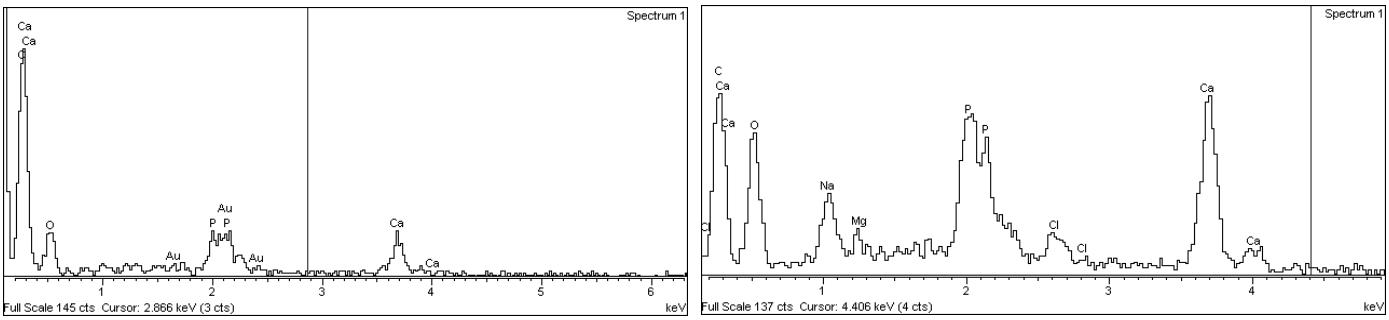

(a) (b)

Figure 9 - EDX spectra of (a) the as-received sample (AR) and (b) a typical CO_2 laser surface modified sample following immersion in SBF after 14 days.

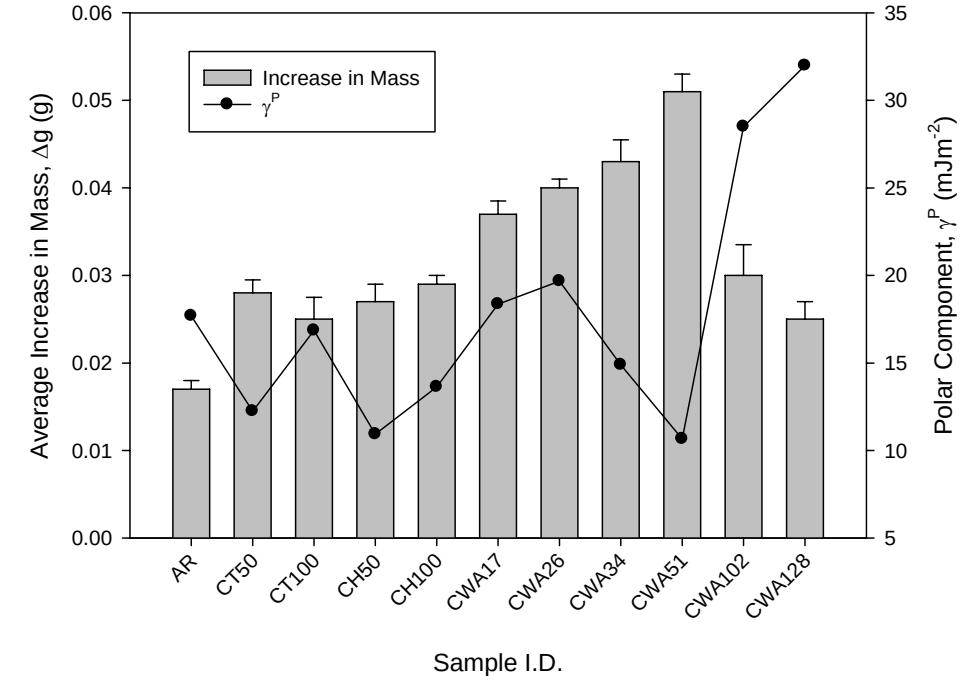

(a)

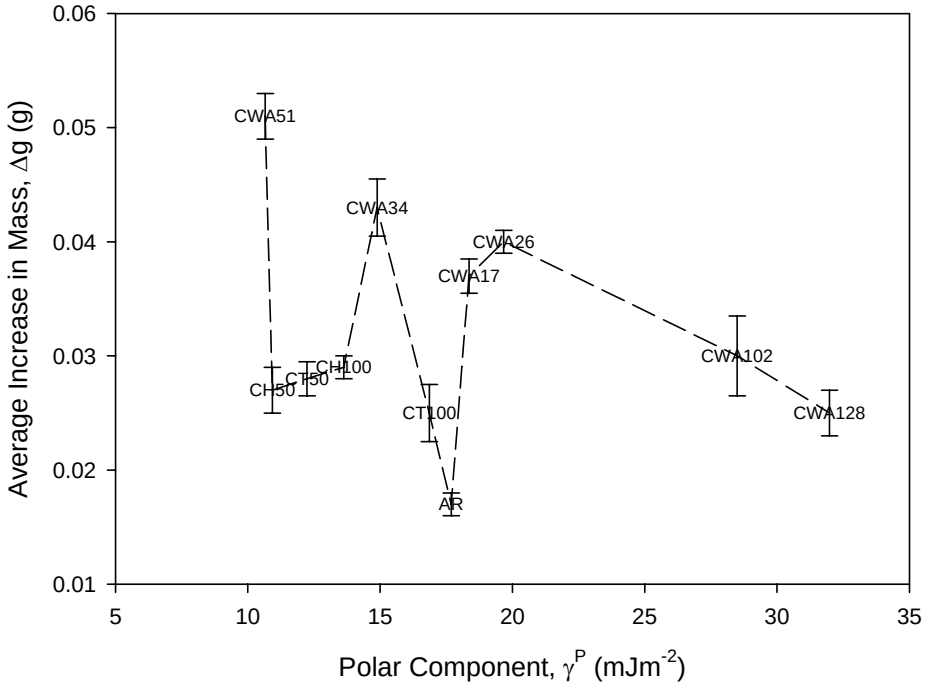

(b)

Figure 10 – (a) Histogram showing the increase in mass, Δg, in relation to γ^P for all CO_2 laser processed samples, (b) Graph showing the relationship between γ^P and Δg for all CO_2 laser processed nylon® 6,6 samples following 14 days immersion in SBF.

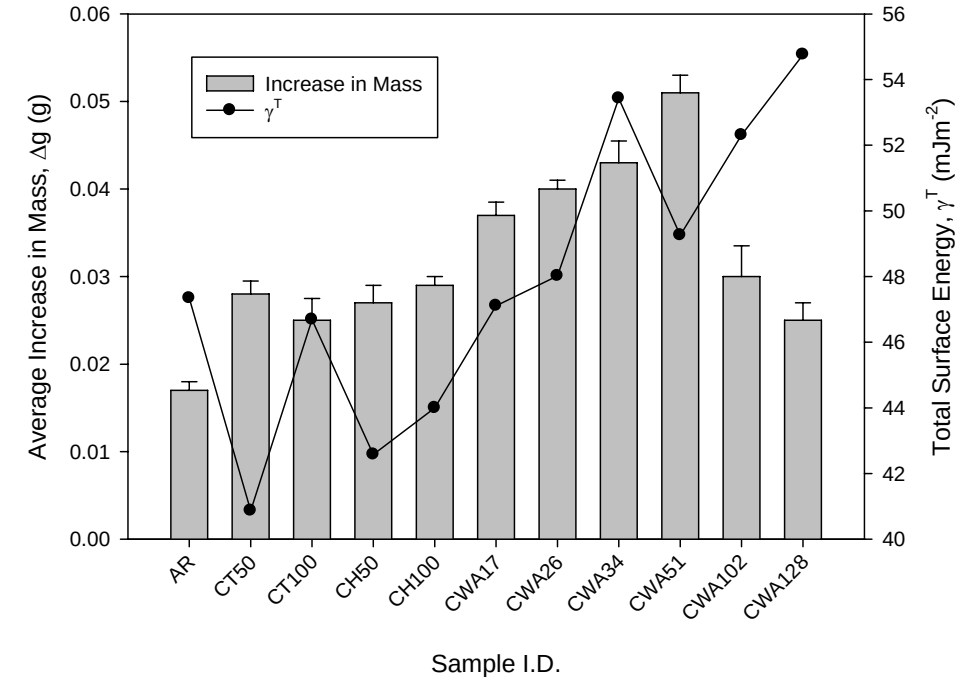

(a)

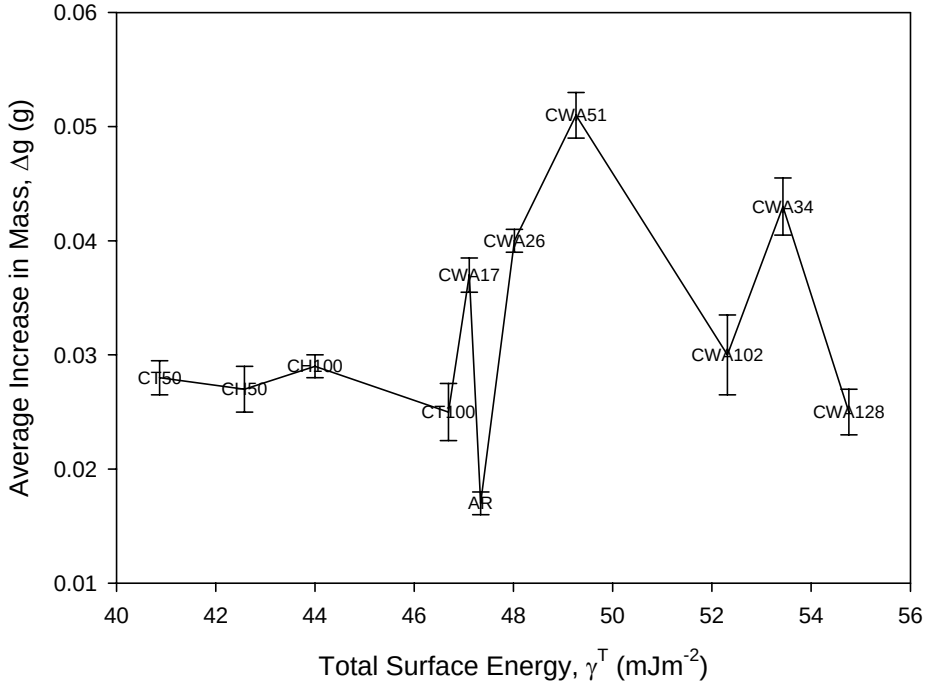

(b)

Figure 11 – (a) Histogram showing the increase in mass, Δg, in relation to γ^T for all CO_2 laser processed samples, (b) Graph showing the relationship between γ^T and Δg for all CO_2 laser processed nylon® 6,6 samples following 14 days immersion in SBF.

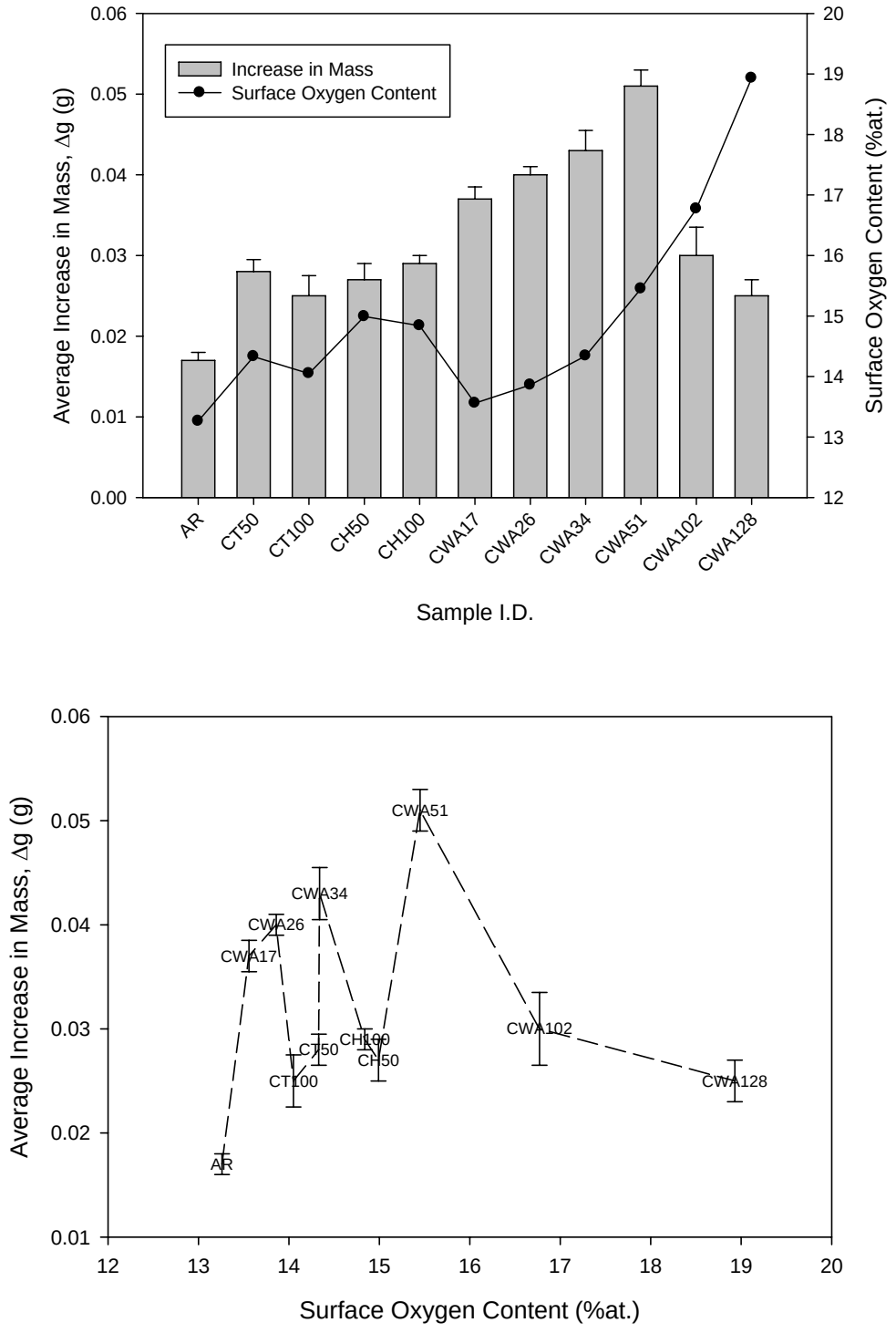

Figure 12 – (a) Histogram showing the increase in mass, Δg, in relation to surface oxygen content for all CO_2 laser processed samples, (b) Graph showing the relationship between surface oxygen content and Δg for all CO_2 laser processed nylon® 6,6 samples following 14 days immersion in SBF.

Table 1 – Results summary for all samples showing roughness parameters, surface oxygen content and wettability characteristics following CO_2 laser processing of nylon® 6,6.

Sample ID	*Sa*	*Ra*	*Polar Component, γ^P*	*Dispersive Component, γ^D*	*Total Surface Energy, γ^T*	*Surface Oxygen Content*	Contact Angle
	(μm)	*(μm)*	*(mJm^{-2})*	*(mJm^{-2})*	*(mJm^{-2})*	*(%at.)*	(°)
AR	0.126	0.029	17.69	29.66	47.34	13.26	56.4±1.2
CO_2 Laser-Induced Patterned Samples							
CT50	0.636	0.148	12.24	28.63	40.87	14.33	66.0±4.0
CT100	0.297	0.185	16.86	29.83	46.69	14.05	57.5±2.4
CH50	0.423	0.103	10.93	31.64	42.58	14.99	65.8±2.9
CH100	0.326	0.155	13.63	30.37	44.00	14.84	62.2±2.3
CO_2 Whole Area Irradiative Processed Samples							
CWA17	0.111	0.060	18.36	28.75	47.11	13.56	55.8±2.7
CWA26	0.100	0.158	19.67	28.35	48.02	13.86	54.6±3.5
CWA34	0.101	0.092	14.89	38.55	53.43	14.34	56.4±3.5
CWA51	0.341	0.139	10.66	38.59	49.26	15.45	64.1±2.2
CWA102	4.356	1.236	28.49	23.82	52.31	16.77	46.6±4.7
CWA128	3.201	1.335	31.98	22.78	54.76	18.93	43.0±3.7